Transfer of Bose-Einstein condensates through discrete breathers in an optical lattice

H. Hennig,[1,2,3,*] J. Dorignac,[3,4] and D. K. Campbell[3]

[1]*Max Planck Institute for Dynamics and Self-Organization, D-37073 Göttingen, Germany*

[2]*Institute for Nonlinear Dynamics, University of Göttingen, D-37073 Göttingen, Germany*

[3]*Boston University, Boston, Massachusetts 02215, USA*

[4]*Laboratoire de Physique Théorique et Astroparticules, CNRS-IN2P3-UMR5207, Université Montpellier 2, F-34095 Montpellier, France*

(Received 17 June 2010; published 4 November 2010)

We study the effect of discrete breathers (DBs) on the transfer of a Bose-Einstein condensate (BEC) in an optical lattice using the discrete nonlinear Schrödinger equation. In previous theoretical (primarily numerical) investigations of the dynamics of BECs in leaking optical lattices, collisions between a DB and a lattice excitation, e.g., a moving breather (MB) or phonon, were studied. These collisions led to the transmission of a fraction of the incident (atomic) norm of the MB through the DB, while the DB can be shifted in the direction of the incident lattice excitation. Here we develop an analytic understanding of this phenomenon, based on the study of a highly localized system—namely, a nonlinear trimer—which predicts that there exists a total energy threshold of the trimer, above which the lattice excitation can trigger the destabilization of the DB and that this is the mechanism leading to the movement of the DB. Furthermore, we give an analytic estimate of upper bound to the norm that is transmitted through the DB. We then show numerically that a qualitatively similar threshold exists in extended lattices. Our analysis explains the results of the earlier numerical studies and may help to clarify functional operations with BECs in optical lattices such as blocking and filtering coherent (atomic) beams.

DOI: 10.1103/PhysRevA.82.053604 PACS number(s): 03.75.Lm, 63.20.Pw, 67.85.De, 42.65.Tg

I. INTRODUCTION

Since the experimental realization of Bose-Einstein condensation (BEC) of ultracold atoms in optical lattices (OLs) [1], many researchers have achieved an extraordinary level of control over BECs in optical traps [2–5]. Among other important applications, this control has allowed for the investigation of analogs of complex solid-state phenomena [6–10]. Technologically, the emerging field of "atomtronics" promises a new generation of nanoscale devices.

An important generic feature of nonlinear lattices is the existence of discrete breathers (DBs), which are spatially localized, time-periodic, stable (or at least long-lived) excitations in spatially extended, perfectly periodic, discrete systems [11–13]. DBs arise intrinsically from the combination of nonlinearity and the discreteness of the system. DBs have been observed in a variety of systems, including Josephson-junction arrays [14,15], micromechanical systems [16], nonlinear waveguide arrays [17,18], α helix proteins [19], spins in antiferromagnetic solids [20,21], and BECs [6]. The existence, stability, and other properties of DBs have been studied theoretically throughout the last decade [13,22–24]. Among other results, it has been demonstrated that DBs act as virtual bottlenecks which slow down the relaxation processes in generic nonlinear lattices [25–28].

Many theoretical studies of the dynamics of a BEC trapped in an OL use the discrete nonlinear Schrödinger equation (DNLS) to model the system. Several recent studies based on the DNLS have observed the collision of a stationary DB with a lattice excitation, e.g., a moving breather or phonon [27–29]. If the amplitude of the lattice excitation is too small, it is reflected entirely from the DB. Above a specific threshold amplitude, part of the incident atomic norm is transmitted through the DB while the DB is destabilized and shifted by one or few lattice sites toward the incoming moving breather (MB).[1] This transmission process plays a central role in the occurrence of scale-free atomic avalanches observed for a whole range of nonlinearities in leaking optical lattices [28]. However, this process has heretofore not been understood analytically.

In this article we analyze, analytically and numerically, the collision process of a stationary DB with a lattice excitation. To this end, we study the nonlinear trimer, i.e., the DNLS with $M = 3$ lattice sites (see, e.g., [5] for an experimental realization of a similar system). We calculate analytically the threshold for the destabilization of the DB as well as an upper bound to the atomic norm that can be transmitted through the DB. The threshold and the transmission process are described by introducing a Peierls-Nabarro energy landscape which restricts the accessible region of the phase excitations on the trimer. The 'local Ansatz', [31,32], an approach applied successfully to studies of DBs on nonlinear lattices, suggests that the results we find for the trimer will apply to extended lattices. For the rather large nonlinearity we shall consider in the sequel, DBs are well localized, and the most basic and important DBs occupy only three sites. Within the local Ansatz we consider only the central site and the two neighboring sites of a DB. This allows us to reduce the high dimensional dynamical problem involving M sites to the nonlinear trimer. A detailed analysis of the reduced problem [31,32] shows that (i) the DB corresponds to a trajectory in the phase space of the full system which is practically embedded on a two-dimensional toroidal manifold, thus being quasiperiodic in time, and (ii) the full DB can be reproduced accurately within the nonlinear trimer

*holgerh@nld.ds.mpg.de

[1]Indications for the migration of a DB by one or a few sites toward a lattice excitation can be found as well in a ϕ^4 nonlinear lattice; see Ref. [30].

approximation. Finally, after having used the trimer to analyze the nature of the transmission process, we establish that the transfer mechanism applies in extended lattices in Sec. VII.

Although we focus here on BECs, our results are also relevant in a wide range of other contexts in which the DNLS applies, most prominently coupled nonlinear optical waveguides [17,18,33–36].

II. MODEL HAMILTONIAN

The Bose-Hubbard Hamiltonian is arguably the simplest model that captures the dynamics of a dilute gas of bosonic atoms in a deep optical lattice, with chemical potential small compared to the vibrational level spacing (see, e.g., [3] for a review). In the case of weak interatomic interactions (superfluid limit) and/or a large number of atoms per well (so that the total number of atoms $N \sim O(10^4$–$10^5)$ is much larger than the number of wells M), a further simplification is available since the BECs dynamics admits a quasiclassical (mean-field) description. The resulting Hamiltonian describing the dynamics is

$$\mathcal{H} = \sum_{n=1}^{M}[U|\psi_n|^4 + \mu_n|\psi_n|^2] - \frac{J}{2}\sum_{n=1}^{M-1}(\psi_n^*\psi_{n+1} + \text{c.c.}), \tag{1}$$

where $n = 1, \ldots, M$ is the index of the lattice site, $|\psi_n(t)|^2 \equiv N_n(t)$ is the mean number of bosons at site n [also referred to as the norm $N_n(t)$], $U = 4\pi\hbar^2 a_s V_{\text{eff}}/m$ describes the interaction between two atoms at a single site (V_{eff} is the effective mode volume of each site, m is the atomic mass, and a_s is the s-wave atomic scattering length), μ_n is the onsite chemical potential, and J is the tunneling amplitude. The "wave functions" ψ_n and $i\psi_n^*$ form conjugate variables leading to a set of canonical equations

$$i\frac{\partial\psi_n}{\partial\tau} = \frac{\partial\mathcal{H}}{\partial\psi_n^*}, \quad i\frac{\partial\psi_n^*}{\partial\tau} = -\frac{\partial\mathcal{H}}{\partial\psi_n}, \tag{2}$$

which upon evaluation yields the discrete nonlinear Schrödinger equation

$$i\frac{\partial\psi_n}{\partial t} = \lambda|\psi_n|^2\psi_n - \frac{1}{2}[\psi_{n-1} + \psi_{n+1}]. \tag{3}$$

Here, $\lambda = 2U/J$ is the nonlinearity and $t = J\tau$ is the normalized dimensionless time. In Eq. (3) we have set $\mu_n = 0\,\forall n$.

The DNLS can be applied to a remarkably large variety of systems, in particular this mathematical model describes (in the mean-field limit) the dynamics of a BEC in an OL of size M [37]. Experimentally, the tunneling rate J can be adjusted by the intensity of the standing laser wave field. A powerful tool to modify the onsite interaction U is via a Feshbach resonance, where the atomic interactions can be controlled over a large range simply by changing a magnetic field. A Feshbach resonance involves the coupling of free unbound atoms to a molecular state in which the atoms are tightly bound. When the energy levels of the molecular state and the state of free atoms come closer, the interaction between the free atoms increases. Thus, the nonlinearity λ can be varied experimentally. Here we will treat the repulsive case explicitly ($\lambda > 0$); however, the attractive case can be obtained via the "staggering" transformation $\psi_n \to (-1^n)\psi_n$ followed by time reversal $t \to -t$ [13].

III. EQUATIONS FOR THE NONLINEAR TRIMER AND ASYMPTOTIC SOLUTIONS

To analyze the transfer of norm through a DB (and the related stability of the DB) during a collision using the nonlinear trimer ($M = 3$), we begin with the equations

$$\begin{aligned} i\partial_t\psi_1 &= \lambda|\psi_1|^2\psi_1 - \tfrac{1}{2}\psi_2, \\ i\partial_t\psi_2 &= \lambda|\psi_2|^2\psi_2 - \tfrac{1}{2}(\psi_1 + \psi_3), \\ i\partial_t\psi_3 &= \lambda|\psi_3|^2\psi_3 - \tfrac{1}{2}\psi_2. \end{aligned} \tag{4}$$

We normalize the wave functions such that the total atomic population reads

$$N = \sum_{n=1}^{M}|\psi_n|^2 = 1.$$

To find single frequency breather solutions in Eq. (4) for the symmetric case $\psi_1 = \psi_3$, we assume

$$\psi_n(t) = A_n e^{iwt}, \tag{5}$$

with amplitudes A_n and frequency w. This ansatz, together with the conservation of particle number, leads to the set of equations

$$\begin{aligned} -wA_1 &= \lambda A_1^3 - \tfrac{1}{2}A_2, \\ -wA_2 &= \lambda A_2^3 - A_1, \\ 1 &= 2A_1^2 + A_2^2. \end{aligned} \tag{6}$$

Let us first calculate the relation between the (atomic) norm $N_2 = A_2^2$ at the central site and the nonlinearity λ. From Eq. (6), we find

$$\lambda(N_2) = \pm\frac{\sqrt{2}(2N_2 - 1)}{\sqrt{N_2(1 - N_2)}(3N_2 - 1)}. \tag{7}$$

We have four solutions above the bifurcation point at $\lambda \approx 5.04$ and two solutions for $0 \leqslant \lambda < 5.04$ (see Fig. 1). To gain further insight into the nature of the symmetric solutions in the trimer, we will revisit Eq. (6), which we convert into a quartic equation

$$x^4 + \frac{\lambda}{\sqrt{2}}x^3 - \sqrt{2}\lambda x - 1 = 0, \tag{8}$$

where

$$A_2 = \cos[\arctan(x)] = \frac{\text{sgn}(x)}{\sqrt{1 + x^2}}. \tag{9}$$

Expansion of the exact real solutions of Eq. (8) in λ for the limiting case $\lambda \to 0$ gives

$$\begin{aligned} x_1 &= 1 + \frac{\lambda}{4\sqrt{2}} - \frac{5}{64}\lambda^2 + O(\lambda^3), \\ x_2 &= -1 + \frac{\lambda}{4\sqrt{2}} + \frac{5}{64}\lambda^2 + O(\lambda^3). \end{aligned} \tag{10}$$

At $\lambda = 0$ the solution $\vec{\psi}(t) = [\psi_1(t), \psi_2(t), \psi_3(t)]$ of Eq. (6) at time $t = 0$ reads $\vec{\psi}_{(x1,x2)}(0) = (1/2, \pm 1/\sqrt{2}, 1/2)$. The antisymmetric breather configuration $\vec{\psi}(0) = (-1/\sqrt{2}, 0, 1/\sqrt{2})$

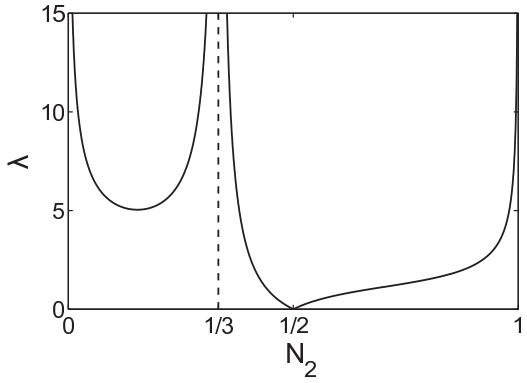

FIG. 1. DB solutions for the symmetric case $\psi_1 = \psi_3$ [Eq. (7)]. For a nonlinearity $\lambda > 5.04$, four symmetric solutions exist. The solution for $N_2 > 1/2$ is termed a bright breather, while the solution for $N_2 \to 0$ corresponds to a dark breather [see Eq. (12)]. The dashed vertical line at $N_2 = 1/3$ marks the asymptote for the phase-wise and antiphase-wise time-periodic solutions for $\lambda \to \infty$.

is not included in our ansatz, as we restrict ourselves to symmetric solutions.

Expansion around the limit $\lambda \to \infty$ leads to four real solutions:

$$\begin{aligned} x_3 &= -\frac{1}{\sqrt{2}}\frac{1}{\lambda} - \frac{1}{4\sqrt{2}}\frac{1}{\lambda^3} + O(\lambda^{-5}), \\ x_4 &= -\frac{1}{\sqrt{2}}\lambda + 2\sqrt{2}\frac{1}{\lambda} + 14\sqrt{2}\frac{1}{\lambda^3} + O(\lambda^{-5}), \\ x_5 &= -\sqrt{2} - \frac{3}{2\sqrt{2}}\frac{1}{\lambda} - \frac{69}{16\sqrt{2}}\frac{1}{\lambda^2} + O(\lambda^{-3}), \\ x_6 &= \sqrt{2} - \frac{3}{2\sqrt{2}}\frac{1}{\lambda} + \frac{69}{16\sqrt{2}}\frac{1}{\lambda^2} + O(\lambda^{-3}). \end{aligned} \tag{11}$$

For infinite λ the solutions of Eq. (6) at time $t = 0$ are

$$\begin{aligned} \vec{\psi}_{(x3)}(0) &= (0,1,0), \\ \vec{\psi}_{(x4)}(0) &= (\sqrt{1/2},0,\sqrt{1/2}), \\ \vec{\psi}_{(x5,x6)}(0) &= (1/\sqrt{3}, \mp 1/\sqrt{3}, 1/\sqrt{3}) , \end{aligned} \tag{12}$$

where the solution $\vec{\psi}_{(x3)}$ is called a bright breather, $\vec{\psi}_{(x4)}$ is named a dark breather (due to lack of norm at the central site), and $\vec{\psi}_{(x5,x6)}$ are phase-wise and antiphase-wise time-periodic solutions.

IV. PEIERLS-NABARRO ENERGY LANDSCAPE

Having found the symmetric DB solutions, we next focus on the transfer of norm through a bright breather, where the stability of the breather will play a crucial role. We start by introducing the concept of a Peierls-Nabarro (PN) energy landscape. It is related to the PN potential, which reflects the fact that discreteness breaks the continuous translational invariance of a continuum model [38,39]. The amplitude of the PN potential may be seen as the minimum barrier which must be overcome to translate an object by one lattice site. Regarding DBs, the Peierls-Nabarro barrier is given by the energy difference $|E_c - E_b|$, where E_c and E_b are the energies of a DB centered at a lattice site and between two lattice sites.

We define the Peierls-Nabarro energy landscape as follows: for a given configuration of amplitudes, A_n, the PN energy landscape is obtained by extremizing H with respect to the phase differences $\delta\phi_{ij} = \phi_i - \phi_j$:

$$H^l_{\rm PN} = \min_{\delta\phi_{ij}}(-H), \quad H^u_{pn} = \max_{\delta\phi_{ij}}(-H), \tag{13}$$

where $\psi_n = A_n \exp(i\phi_n)$ and $H^l_{\rm PN}$ and $H^u_{\rm PN}$ are the lower and upper part of the PN landscape. As we will see later, the bright breather solution $\vec{\psi}_{(x3)}$ is located at an extremum of $H^l_{\rm PN}$. The minus sign in the definition (13) was added for convenience to ensure that the bright breather is found in a minimum (and not in a maximum) of the lower PN landscape. The phase differences extremizing the Hamiltonian

$$\begin{aligned} H = &\frac{\lambda}{2}\left(A_1^4 + A_2^4 + A_3^4\right) \\ &- \left[A_1 A_2 \cos(\phi_1 - \phi_2) + A_2 A_3 \cos(\phi_2 - \phi_3)\right] \end{aligned} \tag{14}$$

are $\delta\phi_{12} = \delta\phi_{23} \in \{0,\pi\}$. Hence, the upper and the lower PN energy landscapes read

$$H^u_{\rm PN} = -\frac{\lambda}{2}\left(A_1^4 + A_2^4 + A_3^4\right) + (A_1 + A_3)A_2, \tag{15}$$

and

$$H^l_{\rm PN} = -\frac{\lambda}{2}\left(A_1^4 + A_2^4 + A_3^4\right) - (A_1 + A_3)A_2 . \tag{16}$$

In Fig. 2 the PN landscape is visualized for $\lambda = 3$. The PN "shell," consisting of the upper and lower landscapes, bounds the phase space of the trimer. Since the DB whose

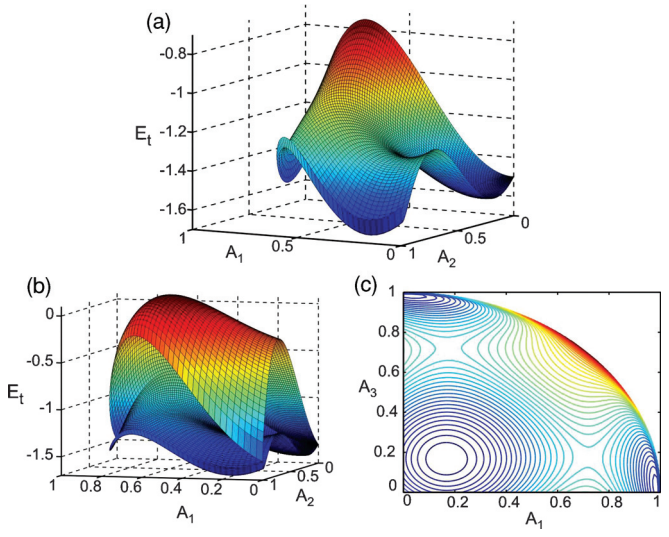

FIG. 2. (Color online) (a) The lower part of the PN energy landscape exhibits three minima separated by saddle points. (b) The phase space of the trimer is restricted to lie between the two parts of the PN shell, which consists of the lower and upper parts of the PN landscape, which are shown in this panel. (c) Contour plot of (a), the lower part of the PN energy landscape. The three minima and saddle points are clearly visible. The minimum at $A_1 = A_3 = 0.17$ in (c) corresponds to the bright breather. The figure is plotted for $\lambda = 3$.

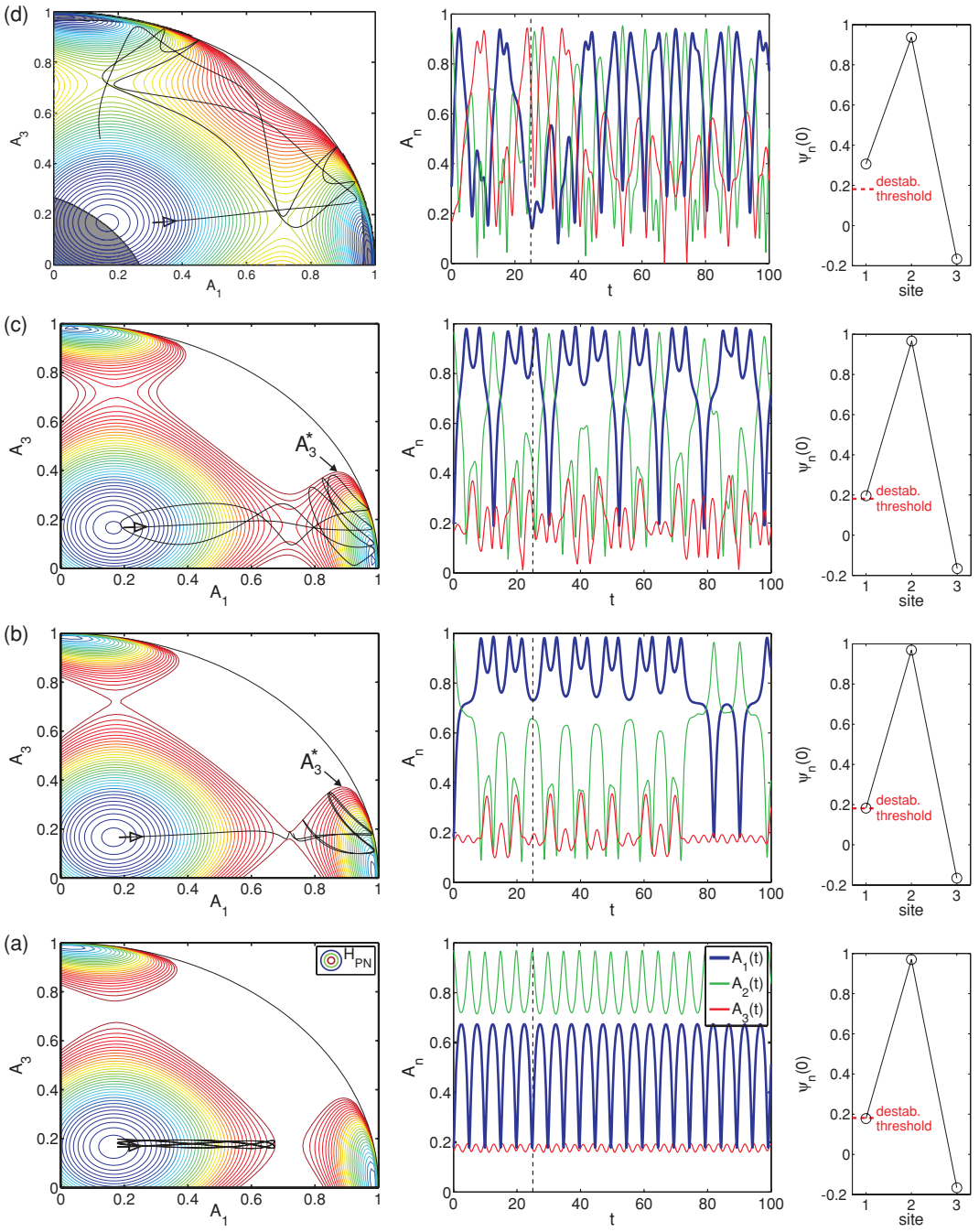

FIG. 3. (Color online) Dynamics on the PN landscape for increasing total energy of the trimer. **(a)** (left) A contour plot of the lower PN energy landscape $H^l_{\rm PN}$ is shown for total energy below the rim ($E_t = -1.32 < E_{\rm thrs} = -1.311$). A projection of the orbit onto the A_1–A_3 plane is over-plotted (black curve). (a) (middle) the corresponding amplitudes $A_i(t)$ indicate that the maximum amplitude remains at the central site. The dashed vertical line marks the time interval [0,25] for which the orbits in the left picture are plotted. (a) (right) A sketch of the initial condition shows that the excitation at site 1 is slightly below threshold. (b) Destabilization of the DB for $E_t = -1.310 > E_{\rm thrs}$ just above the rim. We see that the rim of the PN landscape clearly restricts the dynamics and governs the destabilization process of the DB (left panel). The norm migrates from site 2 to site 1, see the crossing of amplitudes $A_2(t)$ (green/light-gray line) and $A_1(t)$ (blue thick line) for short times $t < 10$ (middle panel). (c) For higher total energy $E_t = -1.28$ the bottleneck at the rim widens and the maximum norm transmitted to site 3 is increased. (d) For even higher total energy $E_t = -1.04$ the orbit explores large parts of the phase space and visits all three sites. The grey shaded area (left panel) is forbidden by the upper PN landscape $H^u_{\rm PN}$. In all cases $\lambda = 3$, $\delta_\phi = \pi$. For other values of δ_ϕ the same qualitative behavior is found.

properties we are studying corresponds to a minimum on $H^l_{\rm PN}$, we shall focus on this landscape. As shown in Fig. 2 (c), the projection onto the A_1-A_3 plane exhibits three minima which are separated by saddle points (called rims in the following). For $\lambda \to \infty$ the saddle points are located at $A_1 = A_2 = \sqrt{1/2}$ (which in the following will be the saddle point of interest)

and $A_2 = A_3 = \sqrt{1/2}$. The energy threshold $E_{\rm thrs}$ at the rim [obtained from Eq. (16)] reads

$$E_{\rm thrs} = -\frac{\lambda}{4} - \frac{1}{2} - \frac{1}{4\lambda} + \frac{1}{4\lambda^2} - \frac{1}{4\lambda^3} + \frac{9}{16\lambda^4} + O(\lambda^{-5}). \tag{17}$$

The following investigation holds for an effective nonlinearity in a range around $\Lambda = \lambda/M \simeq 1$,[2] which is in the critical regime where scale-free avalanches of BECs were found in [28].

V. THRESHOLD FOR TRANSFER OF NORM

To study the influence of the PN landscape on the stability and the transfer of atoms through the DB, we first consider the fixed point corresponding to the bright breather. The initial amplitudes A_i^b are obtained by inverting Eq. (7) for $N_2 > 1/2$; hence an initial condition for the bright breather reads $\vec{\psi}^b(0) = (-A_1^b, A_2^b, -A_1^b)$. Then perturbations are added to site 1. In dynamical systems terminology, the phase space of the trimer is "mixed," consisting of regular islands surrounded by the chaotic sea [28,40]. DBs are located inside the regular islands of the phase space, provided that their frequency (and multiples of their frequency) lie outside the phonon spectrum [31,32]. If a perturbation is large enough, it can push the orbit out of the regular island into the chaotic sea, destabilizing the DB.

We now use the following initial condition:

$$\vec{\psi}(0) = \left[-\left(A_1^b + \delta_A\right)e^{i\delta_\phi}, A_2, -A_1^b\right], \tag{18}$$

where $A_2 = (1 - |\psi_1|^2 - |\psi_3|^2)^{1/2}$ ensures total norm $N = 1$. Compared to the bright breather, we have added an amplitude δ_A to site 1 and the phase ϕ_1 is rotated by δ_ϕ. The initial condition (18) is visualized in Fig. 3 (right panels), where we have fixed $\delta_\phi = \pi$ and increased δ_A in Figs. 3(a)–3(d). Note that although the phase rotation does not alter the norms $|\psi_i|^2$, it drastically changes the total energy of the trimer which we define as $E_t = -H$ [see Eq. (14)].

In Fig. 3 (left) we show the dynamics for increasing total energy E_t, where the arrows on the orbits (black curves) mark the direction of time. For $E_t < E_{\rm thrs}$ the areas in phase space are disconnected, leading to subthreshold dynamics depicted in Fig. 3(a).

In contrast, for $E_t > E_{\rm thrs}$ the orbit is allowed to pass the rim [left panel of Fig. 3(b)]. The majority of the norm migrates from site 2 to site 1 while norm is transferred to site 3. The larger E_t [Fig. 3(c)], the larger is the size of the bubble (by the term "bubble" we denote the accessible region of the PN landscape for $A_1 > 1/\sqrt{2}$). Hence, as we see from Figs. 3(b) and 3(c) (left), an upper limit to the norm that can possibly be transmitted through the DB can be read from the maximum value of A_3 inside the bubble:

$$A_3^* = \max_{A_1 > 1/\sqrt{2}} A_3 \tag{19}$$

for fixed total energy E_t.

Finally, for even larger E_t, the orbit visits large parts of the phase space and large amplitudes $A_i(t)$ are found at all three sites, as depicted in Fig. 3(d), where the orbit resides in the chaotic regime [Fig. 3(d)]. In this case, no controlled shift of the DB from site 2 to 1 is observed and the DB becomes dynamically unstable. These dynamical instabilities can be associated with a (partial) depletion of the BEC [41,42]; a detailed study of these effects is beyond the scope of our present investigation.

The upper bound A_3^* can be calculated analytically noting that for the projection onto the A_1-A_3 plane, condition $dA_3/dA_1 = 0$ holds. Implicit derivation of Eq. (16) leads to

$$0 = 1 - 2A_1^2 - A_1A_3 - A_3^2 + 2\lambda A_1\sqrt{1 - A_1^2 - A_3^2}\left(-1 + 2A_1^2 + A_3^2\right), \tag{20}$$

which determines the maximum value of A_3 in the bubble of the PN landscape as

$$A_3^*(\delta,\lambda) = \frac{1}{\sqrt{2}} - \frac{\sqrt{(1-2\delta)}}{2\sqrt{\lambda}} - \frac{(1-2\delta)}{4\sqrt{2}\lambda} + \frac{1 + 2(\delta - \delta^2)}{4\sqrt{1-2\delta}\lambda^{3/2}} - \frac{25 - 20(\delta - \delta^2)}{64\lambda^2} + \frac{11/8 - 3\delta - \delta^2 + 7(\delta^3 - 7\delta^4)}{2(1-2\delta)^{3/2}\lambda^{5/2}} + O(\lambda^{-3}), \tag{21}$$

where $\delta = E_t - E_{\rm thrs} > 0$ is the energy relative to the destabilization threshold. Without the $\lambda^{-5/2}$ term the exact value is

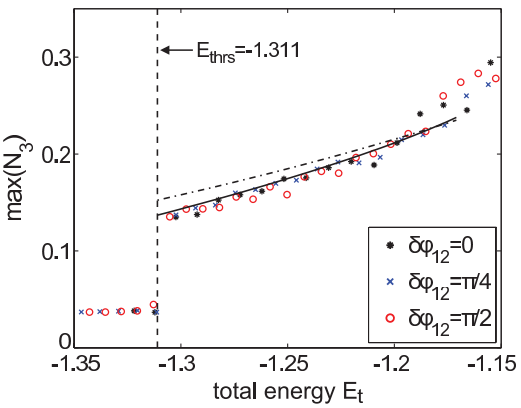

FIG. 4. (Color online) Norm transfer through a bright breather. The maximum (atomic) norm at site 3 detected after the collision of the DB with a lattice excitation is shown as a function of the total energy of the trimer. The discrete symbols indicate three different values of the initial phases. For $E_t < E_{\rm thrs}$ the DB is stable and practically no transfer of norm takes place on short time scales. For $E_t > E_{\rm thrs}$ we observe instability of the DB centered at site 2: the breather migrates to site 1 and norm is transferred to site 3. An upper bound to $\max[N_3(t)]$ is calculated from the PN landscape, both analytically [dotted dashed line, cf. Eq. (21)] and umerically (solid line). The analytical calculation is performed in the limit for large λ and therefore deviates slightly from the exact numerical result. We used $\delta\phi_{23} = \pi$ which is the typical case observed in [28] for DBs in an extended leaking optical lattice and $\lambda = 3$.

[2]For nonlinearities $\Lambda \ll 1$, no such saddle points in the PN landscape are found.

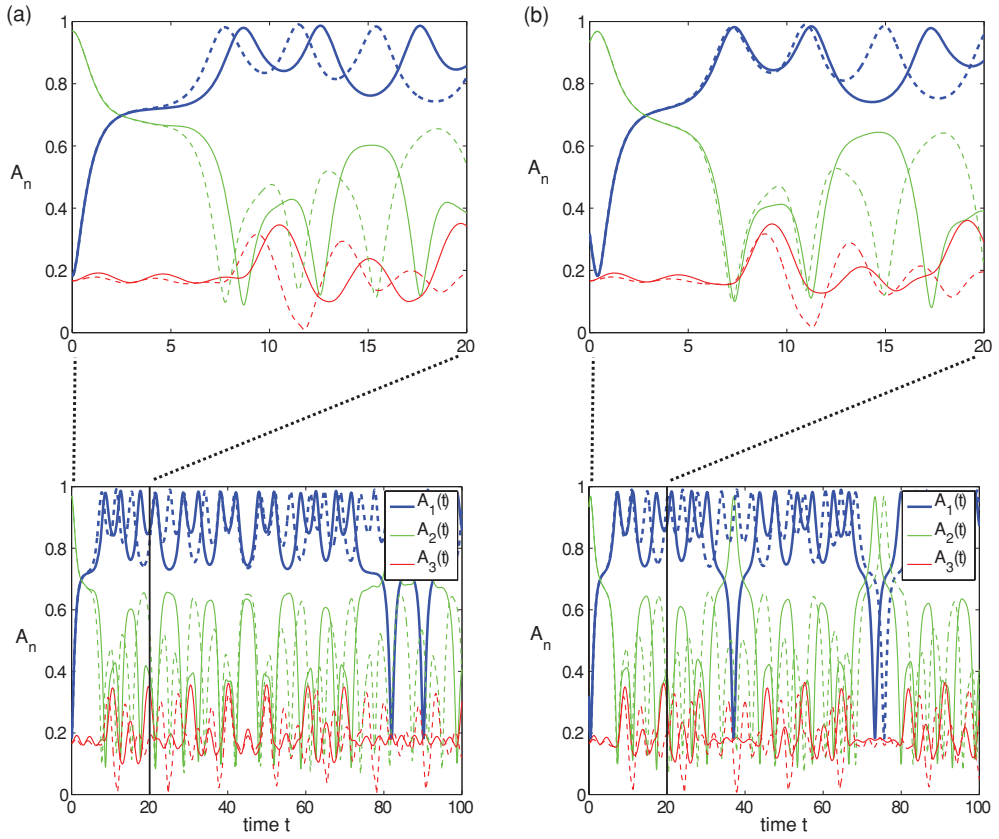

FIG. 5. (Color online) The destabilization of the DB in the trimer (solid lines) is compared to the trimer with a third linear site (dashed lines). On the time scale, where the destabilization takes place, the dynamics is qualitatively very similar—see enlargements in upper pictures showing a crossing of $A_2(t)$ (green/light-gray line) and $A_1(t)$ (blue thick line) at $t \approx 2.5$. Total energy is $E_t = -1.31 > E_{\text{thrs}}$ and $\lambda = 3$. (a) The initial condition (18) is given by $\delta A = 0.016$, $\delta_\phi = \pi$, which is the same as in Fig. 3(b). (b) The initial condition is determined by the parameters $\delta A = 0.152$, $\delta_\phi = \pi/2$.

underestimated. If we truncate the expression after the $\lambda^{-3/2}$ term, the deviation from the exact result roughly doubles compared to what is shown in Fig. 4.

How general is the transfer mechanism that we describe? In Fig. 4, the maximum norm N_3 that is found at site 3 after the transfer of atoms through the DB is shown as a function of the total energy for three initial phase differences $\delta\phi_{12} = \pi - \delta_\phi = 0, \pi/4, \pi/2$. The dashed vertical line at $E_t = E_{\text{thrs}} = -1.311$ marks the total energy at the rim and is identified with the destabilization threshold of the DB. Evidently, the transfer mechanism found does not depend on parameters δ_A and δ_ϕ individually, but rather on the total energy which determines the accessible region of the PN landscape. Moreover, the transfer mechanism itself appears nearly independent of the choice of the initial phase difference $\delta\phi_{12}$. The maximum norm detected at site 3 is closely below the upper bound $N_3^*(\delta) = |A_3^*(\delta)|^2$ given by Eq. (21), which holds for $E_t \lesssim -1.2$. For increasing $E_t \gtrsim -1.2$ the fluctuations of $\max(N_3)$ for different orbits with similar total energy become larger, because the orbits explore a larger part of the phase space. As a consequence, $\max_{t<T}[N_3(t)]$ depends on the chosen time interval $[0,T]$ in which the maximum norm is detected. (In all cases we set $T = 100$.) In contrast, for lower total energy where a nontrivial upper-bound $N_3^*(\delta)$ of the transferred norm holds, $\max_{t<T}[N_3(t)]$ does barely depend on T already after very few oscillations of $A_3(t)$ [cf. Figs. 3(b) and 3(c) (middle)].

VI. CONNECTION TO PN BARRIER

To gain further insight into the relation between the rim of the PN energy landscape and the PN barrier, let us consider a nonlinear trimer where we omit the nonlinear onsite interaction term at site 3. The equations of motion read

$$\begin{aligned} i\,\partial_t \psi_1 &= \lambda|\psi_1|^2\psi_1 - \tfrac{1}{2}\psi_2, \\ i\,\partial_t \psi_2 &= \lambda|\psi_2|^2\psi_2 - \tfrac{1}{2}(\psi_1 + \psi_3), \\ i\,\partial_t \psi_3 &= -\tfrac{1}{2}\psi_2\,. \end{aligned} \tag{22}$$

Using the initial condition (18), we find that on the time scale where the destabilization process of the DB centered at site 2 takes place, the dynamics is not changed substantially compared to the results for the nonlinear trimer (see Fig. 5). Hence, in order to describe the destabilization of the DB (and the basic mechanism of the norm transfer through the DB), it is sufficient to consider only two nonlinear sites with a third linear site attached. This is a strong indication that the destabilization threshold during the collision of the two objects can actually be linked to the Peierls-Nabarro barrier of a *single* DB.

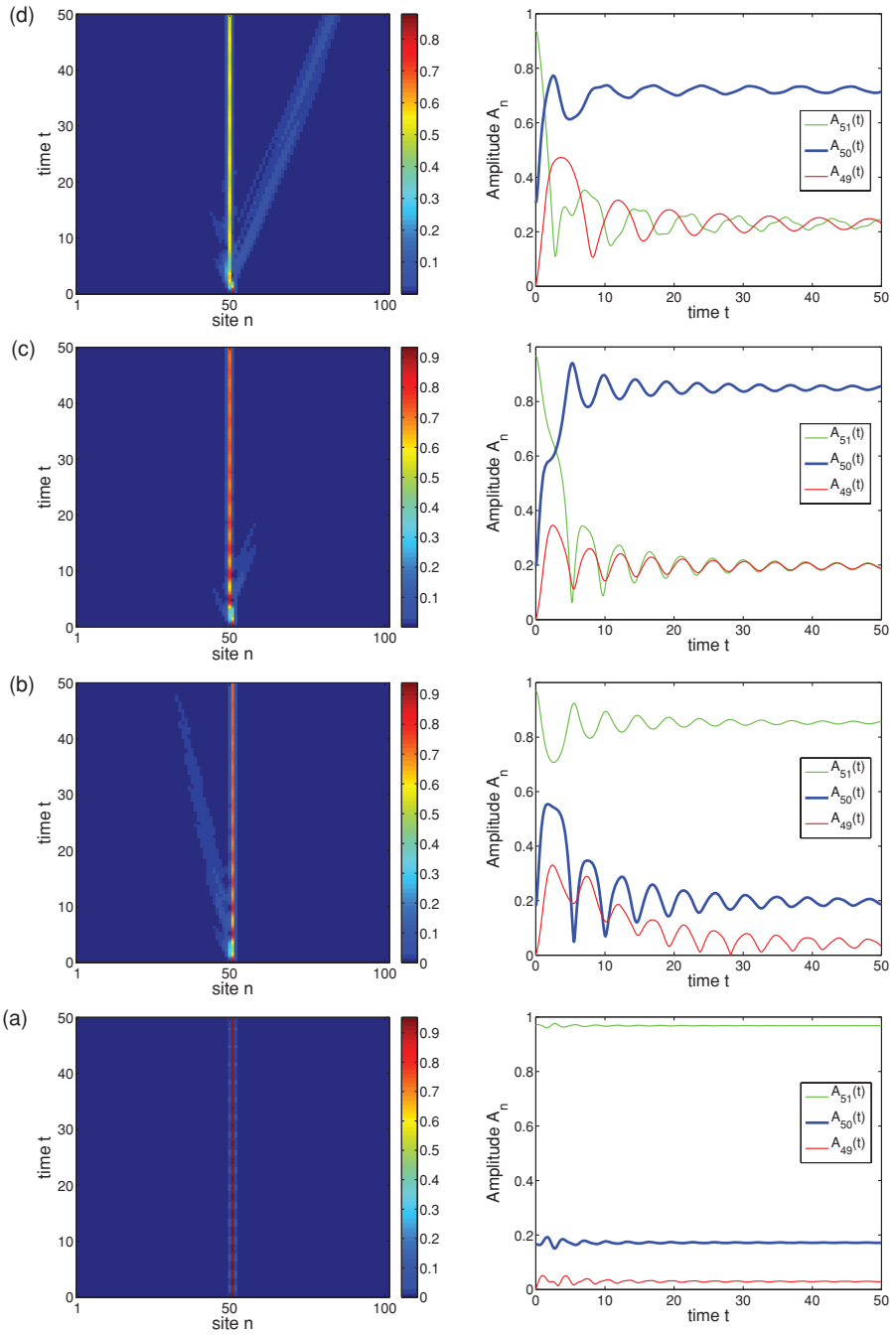

FIG. 6. (Color online) Demonstration that the proposed mechanism for the destabilization and migration of a DB works in an extended lattice ($M = 101$ wells). (a) Unperturbed breather solution from the trimer centered in the middle of the lattice at site 51. The color code represents the (atomic) norm $|\psi_n(t)|^2$ (left panel). In the right panel the amplitudes of the central site of the initial breather, A_{51} (green/light-gray line), and the two neighbors to the left, A_{50} (blue thick line) and A_{49} (red line), are monitored. (b)–(d) Increasing perturbation at the left neighboring site $n = 50$. (b) The total energy of the local trimer $(\psi_{c-1}, \psi_c, \psi_{c+1})$ is just above E_{thrs}. The breather is barely stable but no migration takes place. (c) The breather migrates by one site toward the perturbation (that is, to the left) after $t \approx 5$ time steps. (d) During the migration process, a moving breather is initiated to the right. For $t > 5$ the right panel of (c) and (d) monitors a local trimer, with the breather having moved into its center. Initial conditions are given by Eq. (23) with (a) $\delta_A = \delta_\phi = 0$, (b) $\delta_A = 0.016$, $\delta_\phi = \pi$, (c) $\delta_A = 0.03$, $\delta_\phi = \pi$, and (d) $\delta_A = 0.14$, $\delta_\phi = \pi$.

VII. EXTENDED LATTICES

Having analyzed the nature of the transmission process in the trimer, we now test the general transfer mechanism in extended lattices ($M > 3$). As a proof of principle, we use the same initial conditions as in Figs. 3(b)–3(d) and nonlinearity $\lambda = 3$ to initiate a perturbed trimer above the destabilization threshold in the middle of an otherwise empty lattice of $M = 101$ sites. Denoting the central site of the discrete breather as c (here: $c = 51$), the initial condition reads

$$\psi_{c-1}(0) = -\left(A_1^b + \delta_A\right)e^{i\delta_\phi}, \quad \psi_c(0) = A_2,$$
$$\psi_{c+1}(0) = -A_1^b, \quad \psi_n(0) = 0, \text{ else}, \tag{23}$$

where $A_2 = (1 - |\psi_{c-1}|^2 - |\psi_{c+1}|^2)^{1/2}$ and A_1^b is obtained exactly as we did for Eq. (18). Using initial condition (23), the wave function is normalized to $||\psi||^2 = 1$.

In Fig. 6(a) the analytical solution for the bright breather in the trimer [i.e., initial condition (23) with $\delta_a = \delta_\phi = 0$] is inserted in an extended lattice. We see that initial oscillations of the amplitudes $A_c(t)$, $A_{c-1}(t)$, and $A_{c+1}(t)$ are damped (right panel), approaching a fixed point. For convenience, we have chosen an uneven number of lattice sites M, so that $A_{50}(t) = A_{52}(t)$ and $A_{49}(t) = A_{53}(t)$, etc., at all times (for this symmetric initial condition).

When perturbing the breather at site $c - 1$ (from the left) just above threshold, in contrast to the dynamics in the trimer, we find that the breather is not shifted as in Fig. 3(b), but

remains barely stable, see Fig. 6(b). The reason is that energy can flow into additional degrees of freedom that are present in extended lattices [see the population of site $A_{49}(t)$ for short times $t < 10$]. For larger perturbations, however, the breather is destabilized as expected [cf. Figs. 6(c) and (d) and Figs. 3(c) and (d)]. For large perturbations [Fig. 6(d)], a moving breather is initiated in the course of the migration process, which travels to the right toward the boundary.

These results confirm that up to a precise determination of the destabilization threshold (which is slightly higher on the extended lattice than on the trimer), the general mechanism for the destabilization and migration of a DB also applies to extended lattices.

VIII. POSSIBLE APPLICATIONS

To begin, we should comment on the validity of the DNLS (3) to describe actual experiments of BECs in OLs. Experimental realizations have been performed for values of $\lambda = 2U/J$ in the range 10^{-5}–10^{-3}, while the number of atoms is typically $N \sim O(10^4$–$10^5)$. These estimations lead to experimentally feasible parameters $\Lambda = \lambda/M \lesssim 1$ for which the DNLS is a good approximation. For example, the experiment of [8] shows that the BEC dynamics in an OL with parameters $N \approx 2 \times 10^5$, $J = 0.14E_R, 2UN \approx 12E_R$ [where $E_R = \hbar^2 k_L^2/(2m)$ is the recoil energy and k_L is the laser mode which traps the atoms], and $M = 200$ wells is described very well by the DNLS with effective nonlinearity $\Lambda \approx 0.5$.

To estimate the minimum duration of an experiment with BECs probing the destabilization process, we rewrite our dimensionless time $t = J\tau$ in terms of real time τ. Typical values for J are taken from [43]: the Josephson energy $E_J/k_B = 378\,\mathrm{nK}$ leads to the tunneling rate $J/\hbar = E_j(N\hbar)^{-1} = 16.5\,\mathrm{Hz}$ (for $N = 3000$ atoms). Hence, with these parameters, $t = 10$ (which is a typical time scale after which the destabilization process took place) relates to $\tau \approx 0.6\,\mathrm{s}$.

The thresholded transfer of norm through a bright breather that we analyzed may lead to interesting applications for blocking and filtering atom beams. It could be a powerful tool for controlling the transmission of matter waves in interferometry and quantum-information processes [44].

In a similar way, our findings can be related to the field of optics, because the DNLS is capable of describing wave motion in nonlinear optical waveguide arrays. Discrete breathers in such two-dimensional networks have been investigated in recent years both theoretically and experimentally [17,18,33–36,45,46] and can exhibit a rich variety of functional operations such as blocking, routing, or logic functions [34,35]. Experimental evidence of the destabilization process of the stationary DB should be observable in nonlinear waveguide arrays and might lead to functional operations such as filtering optical beams. Moreover, in view of a molecular trimer, applications in terms of targeted energy transfer (introduced in [47,48]) with a threshold are conceivable, e.g., in the field of biophysics or biomolecular engineering.

IX. CONCLUSIONS

We have found an analytic description of the destabilization threshold and the norm transfer through a DB in extended OL by studying analytically the highly localized case of the nonlinear trimer. A key element was the definition of the two-dimensional Peierls-Nabarro energy landscape. The PN landscape restricts the dynamics of the trimer and the accessible region of the phase space. This restriction of the dynamics becomes very pronounced at the destabilization threshold, which is identified with a rim in the PN landscape. The effect is found for a broad range of the phase differences $\delta\phi_{12}$ between possible colliding objects. Our numerical results confirm that this mechanism also occurs in extended lattices. We discuss some potential applications to experimental systems.

ACKNOWLEDGMENTS

The authors thank Boston University, where the bulk of this work was done, for hospitality and support. One of us (D.K.C.) thanks the Max Planck Institute for Dynamics and Self-Organization for hospitality during the initial stages of the project and the Aspen Center for Physics for hospitality during the completion of the work. We gratefully acknowledge useful conversations with Theo Geisel, Ragnar Fleischmann, and Cristiane de Morais Smith.

[1] M. H. Anderson, J. R. Ensher, M. R. Matthews, C. E. Wieman, and E. A. Cornell, Science **269**, 198 (1995).
[2] O. Morsch and M. Oberthaler, Rev. Mod. Phys. **78**, 179 (2006).
[3] I. Bloch, J. Dalibard, and W. Zwerger, Rev. Mod. Phys. **80**, 885 (2008).
[4] T. Gericke, P. Würtz, D. Reitz, T. Langen, and H. Ott, Nature Phys. **4**, 949 (2008).
[5] J. Estève, C. Gross, A. Weller, S. Giovanazzi, and M. K. Oberthaler, Nature (London) **455**, 1216 (2008).
[6] B. Eiermann, T. Anker, M. Albiez, M. Taglieber, P. Treutlein, K.-P. Marzlin, and M. K. Oberthaler, Phys. Rev. Lett. **92**, 230401 (2004).
[7] I. Carusotto and G. C. LaRocca, Phys. Rev. Lett. **84**, 399 (2000).
[8] F. S. Cataliotti, S. Burger, C. Fort, P. Maddaloni, F. Minardi, A. Trombettoni, A. Smerzi, and M. Inguscio, Science **293**, 843 (2001).
[9] M. Greiner, O. Mandel, T. Esslinger, T. W. Hänsch, and I. Bloch, Nature (London) **415**, 39 (2002).
[10] T. Schumm, S. Hofferberth, L. M. Andersson, S. Wildermuth, S. Groth, I. Bar-Joseph, J. Schmiedmayer, and P. Krüger, Nature Phys. **1**, 57 (2005).
[11] D. K. Campbell, S. Flach, and Y. S. Kivshar, Phys. Today **57**, 43 (2004).
[12] D. K. Campbell, Nature (London) **432**, 455 (2004).
[13] S. Flach and A. V. Gorbach, Phys. Rep. **467**, 1 (2008).

[14] E. Trias, J. J. Mazo, and T. P. Orlando, Phys. Rev. Lett. **84**, 741 (2000).
[15] A. V. Ustinov, Chaos **13**, 716 (2003).
[16] M. Sato, B. E. Hubbard, A. J. Sievers, B. Ilic, D. A. Czaplewski, and H. G. Craighead, Phys. Rev. Lett. **90**, 044102 (2003).
[17] H. S. Eisenberg, Y. Silberberg, R. Morandotti, A. R. Boyd, and J. S. Aitchison, Phys. Rev. Lett. **81**, 3383 (1998).
[18] R. Morandotti, U. Peschel, J. S. Aitchison, H. S. Eisenberg, and Y. Silberberg, Phys. Rev. Lett. **83**, 2726 (1999).
[19] A. Xie, L. van der Meer, W. Hoff, and R. H. Austin, Phys. Rev. Lett. **84**, 5435 (2000).
[20] U. T. Schwarz, L. Q. English, and A. J. Sievers, Phys. Rev. Lett. **83**, 223 (1999).
[21] M. Sato and A. J. Sievers, Nature (London) **432**, 486 (2004).
[22] S. Aubry, Physica D **103**, 201 (1997).
[23] A. R. Bishop, G. Kalosakas, K. Ø. Rasmussen, and P. G. Kevrekidis, Chaos **13**, 588 (2003).
[24] J. Dorignac, J. C. Eilbeck, M. Salerno, and A. C. Scott, Phys. Rev. Lett. **93**, 025504 (2004).
[25] G. P. Tsironis and S. Aubry, Phys. Rev. Lett. **77**, 5225 (1996).
[26] K. Ø. Rasmussen, S. Aubry, A. R. Bishop, and G. G. Tsironis, Eur. Phys. J. B **15**, 169 (2000).
[27] R. Livi, R. Franzosi, and G.-L. Oppo, Phys. Rev. Lett. **97**, 060401 (2006).
[28] G. S. Ng, H. Hennig, R. Fleischmann, T. Kottos, and T. Geisel, New J. Phys. **11**, 073045 (2009).
[29] R. Franzosi, R. Livi, and G.-L. Oppo, J. Phys. B **40**, 1195 (2007).
[30] M. V. Ivanchenko, O. I. Kanakov, V. D. Shalfeev, and S. Flach, Physica D **198**, 120 (2004).
[31] S. Flach and C. R. Willis, Phys. Lett. A **181**, 232 (1993).
[32] S. Flach and C. R. Willis, Phys. Rep. **295**, 181 (1998).
[33] D. Hennig and G. P. Tsironis, Phys. Rep. **307**, 333 (1999).
[34] D. N. Christodoulides and E. D. Eugenieva, Phys. Rev. Lett. **87**, 233901 (2001).
[35] D. N. Christodoulides, F. Lederer, and Y. Silberberg, Nature (London) **424**, 817 (2003).
[36] T. Kottos and M. Weiss, Phys. Rev. Lett. **93**, 190604 (2004).
[37] A. Trombettoni and A. Smerzi, Phys. Rev. Lett. **86**, 2353 (2001).
[38] Y. S. Kivshar and D. K. Campbell, Phys. Rev. E **48**, 3077 (1993).
[39] B. Rumpf, Phys. Rev. E **70**, 016609 (2004).
[40] S. Mossmann and C. Jung, Phys. Rev. A **74**, 033601 (2006).
[41] F. Trimborn, D. Witthaut, and H. J. Korsch, Phys. Rev. A **79**, 013608 (2009).
[42] F. Trimborn, D. Witthaut, and H. J. Korsch, Phys. Rev. A **77**, 043631 (2008).
[43] R. Gati, J. Esteve, B. Hemmerling, T. B. Ottenstein, J. Appmeier, A. Weller, and M. K. Oberthaler, New J. Phys. **8**, 189 (2006).
[44] R. A. Vicencio, J. Brand, and S. Flach, Phys. Rev. Lett. **98**, 184102 (2007).
[45] Y. S. Kivshar, Opt. Lett. **18**, 1147 (1993).
[46] J. Meier, G. I. Stegeman, Y. Silberberg, R. Morandotti, and J. S. Aitchison, Phys. Rev. Lett. **93**, 093903 (2004).
[47] G. Kopidakis, S. Aubry, and G. P. Tsironis, Phys. Rev. Lett. **87**, 165501 (2001).
[48] G. P. Tsironis, Chaos **13**, 657 (2003).